

Vibration analysis and topology optimization of the header of full-feeding rice combine harvester

Han Tang¹, Changsu Xu¹, Jianhua Zhu¹, Rui Guan², Jinwu Wang^{1*}

(1. College of Engineering, Northeast Agricultural University, Harbin 150030, China;

2. School of Water Conservancy and Civil Engineering, Northeast Agricultural University, Harbin 150030, China)

Abstract: The header frame of full-feeding rice combine harvester was characterized by severe vibration due to the excitation force generated by the movement of each working part. In order to solve the problem, the parametric model of the header frame was established, and the accuracy of the finite element model was verified by comparison of the results of the free modal analysis and free vibration modal test based on Eigensystem Realization Algorithm (ERA). Then the constrained modal frequencies were calculated and compared with the external excitation source frequencies, the results showed that the first and eighth order modal natural frequencies were coupled with the excitation frequencies of the threshing cylinder and the engine respectively, which were apt to resonate. To avoid resonance and achieve lightweight design, topology optimization, and finite element analysis were carried out. The optimization results showed that the strength and rigidity meet the requirements and the weight was 14.17% lower than before. The first and eighth order modal natural frequencies were far away from the excitation frequencies range of the threshing cylinder and engine, and the frequencies were far away from the range of each excitation frequency, which effectively avoided the occurrence of resonance. Field experiments showed that the peak value of the vibration acceleration in the three directions of the 8 measuring points of the optimized header frame was significantly reduced, which effectively reduced the vibration of the header frame during harvest. This study provides a method for obtaining the vibration characteristics of key components of agricultural machinery and provides a reference for the weight and vibration reduction of header frames of rice, wheat, rape, and other crop combine harvesters.

Keywords: eigensystem realization algorithm, modal analysis, free modal test, topology optimization, lightweight, field experiment

DOI: [10.25165/j.ijabe.20231604.7096](https://doi.org/10.25165/j.ijabe.20231604.7096)

Citation: Tang H, Xu C S, Zhu J H, Guan R, Wang J W. Vibration analysis and topology optimization of the header of full-feeding rice combine harvester. *Int J Agric & Biol Eng*, 2023; 16(4): 96–108.

1 Introduction

Rice is one of the most important food crops in the world, and its production plays a vital role in ensuring global food security and economic stability. China's rice cultivation area reaches 30 million hm², and its output accounts for about 40% of the country's total grain output. In 2020, the comprehensive mechanization level of rice reached 85.0%. As the key link in the entire mechanization of rice production, harvest has reached 93.1%^[1]. Mechanized harvesting mainly has two methods: segmented harvesting and combined harvesting^[2], and the segmented harvesting method is gradually replaced by the combined harvesting method which saves labor and time. The full-feeding combine harvester is widely used in China because of its high production efficiency and strong adaptability. As one of the most critical working parts, the header has the function of picking, cutting, and conveying. Its reliability directly affects the level of subsequent threshing, cleaning, and

other processes. The header frame is the main bearing cavity of reel, auger, cutter, and other working parts, which plays the role of fixation, support, and protection. Because the frame is subject to vibrated by multi-source excitation, which directly affects the reliability of the whole machine and the harvesting effect^[3].

The application of vibration response characteristics in the field of agricultural machinery provided a reference for the development of some fruit harvesters^[4-8], but the vibration was harmful to mechanical components in most cases. Aiming at the problems of violent vibration, low reliability, and bad comfort in the operation of agricultural machinery, many scholars have made a lot of research on mechanical theory, simulation analysis, vibration detection, optimization design, etc. Zou et al.^[9] found that there was a correlation between structural mode and vibration. With the application of computer technology, finite element analysis software is widely used in structural modal analysis. Bajoria et al.^[10] conducted a free modal analysis on the cold-bent frame using ANSYS and its vibration characteristics were obtained. Kumar et al.^[11] built the parametric model of vehicle gearbox components and conducted modal analysis to obtain the natural frequency and mode. An effective method for studying the vibration of key components of agricultural machinery was provided by the modal analysis, but the vibration characteristics of the mechanical structure cannot be accurately obtained by software simulation alone. Jin et al.^[12] obtained the vibration characteristics of vehicle-mounted spray based on modal test, and verified the excitation characteristics of different combined modal shapes. The research of the above scholars only explored the vibration characteristics of mechanical

Received date: 2021-12-09 **Accepted date:** 2022-12-31

Biographies: Han Tang, PhD, Associate Professor, research interest: related mechanism of seed metering device, Email: tanghan@neau.edu.cn; Changsu Xu, PhD, research interest: loss reduction method of combined harvest, Email: ChangsuXu@neau.edu.cn; Jianhua Zhu, Master, research interest: key technology and equipment for rice combined harvesting, Email: huazai423@126.com; Rui Guan, Master, Laboratory assistant, interest: reliability engineering of agricultural machinery, Email: GuanRui@neau.edu.cn.

***Corresponding author:** Jinwu Wang, PhD, Professor, research interest: reliability engineering of agricultural machinery. College of Engineering, Northeast Agricultural University, Harbin 150030, China. Tel: +86-451-55190950, Email: jinwuw@neau.edu.cn.

structures by means of single software simulation or single free mode test, and did not organically combine the two, which cannot verify the accuracy of finite element model establishment, and cannot provide accurate data reference for later optimization design. The free modal test results are the vibration characteristics of mechanical structure without additional constraints, some scholars have found that the modal test with constraints on the structure according to the actual situation can better match the modal results^[13]. However, there will be significant dynamic coupling between the structure and the working parts that need to be solved in the process of constrained modal test, and the application of vibration isolation device between them will destroy the actual constrained state, so the accurate structural vibration characteristics cannot be obtained^[14].

The purpose of obtaining the vibration characteristics of structure was to reduce the occurrence of vibration. Most of the studies aimed at reducing the vibration of tractors to improve driving comfort. Deboli et al.^[15] conducted experimental research on agricultural tractor seats with different surfaces and configurations to obtain the transfer rate of the seats in three orthogonal directions, providing reference for reducing cab vibration and improving comfort. Deprezk et al.^[16] and Cheng et al.^[17] reduced the impact of vibration by changing the structural parameters of the suspension, and effectively improved the driving comfort of the tractor. In view of the multi-excitation sources and complex vibration of the combine harvester, the research focused on the vibration reduction of key components. Jiang et al.^[18] effectively reduced the resonance of rape mower frame by increasing the arch structure of the frame. Li et al.^[19] optimized the parameters of combine harvester header frame and increased the counterweight of cutter crankshaft to effectively reduce the vibration amplitude. Most of the above researches were designed to reduce vibration by adding vibration-isolating plates, reinforcing beams, and other weight-increasing forms, which can effectively reduce the vibration of the structure while increasing the quality of the structure, but cannot achieve the purpose of reducing the weight of the structure while ensuring mechanical performance.

The optimization methods of key components are mostly focused on shape optimization and size optimization, but topology optimization with larger design space and higher efficiency than that is gaining more and more attention^[20]. Topology optimization uses the given design domain, constraints, and load conditions to determine whether there are cavities in the structure, the number and location of cavities, and other topological forms. It divides the region into enough sub-regions and analyzes the structure. At the same time, according to some optimization strategies and criteria, it deletes some elements from the sub-regions, describes the optimal topology of the structure with the remaining elements, and the modal frequency can be changed to avoid resonance by changing the mass and stiffness distribution of the structure. Xu et al.^[21] reduced the quality of stamping die for high-strength steel of automobiles through topology optimization, and ensured the forming performance of stamping parts by using the die. Kim et al.^[22] carried out topology optimization on the rear suspension of the vehicle to improve the ride comfort and handling stability of the vehicle. Qin et al.^[23] proposed a topology optimization design method for metamaterials, the vibration reduction performance of the new metamaterials was 12% higher than that of the traditional honeycomb materials. Stanford et al.^[24] carried out topology optimization on the structural parameters of the aircraft blades to solve the aeroelastic flutter problem of the aircraft blades. Topology

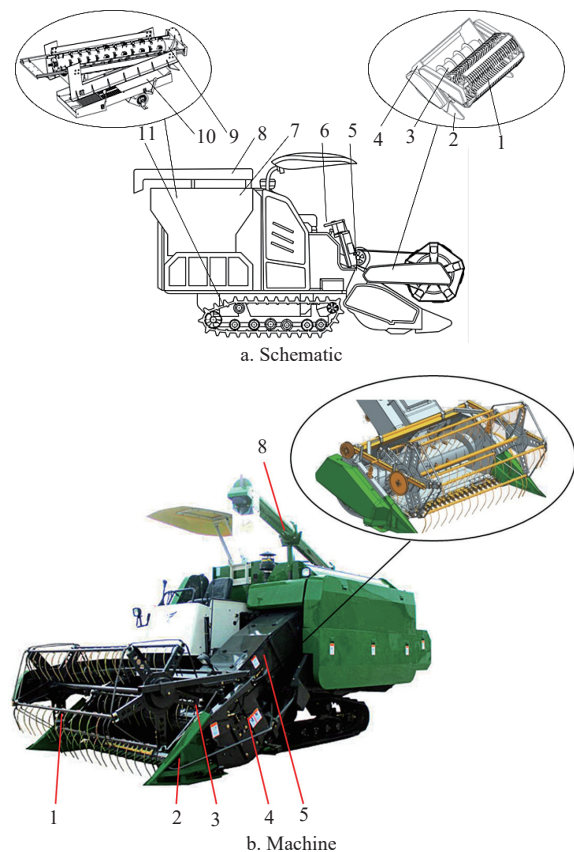
optimization has become a hot topic in optimization methods.

In view of that, this paper made an in-depth analysis of the vibration characteristics of the header frame of a full-feeding rice combine harvester. The accuracy of the model was verified by establishing the parameterized model of the header frame, combined with free modal analysis and modal test. The vibration characteristics of the header frame were obtained by constrained modal analysis, and the excitation sources that affect the resonance were explored. The solution was based on the topological optimization method from the perspective of lightweight to solve the resonance problem caused by the vibration coupling between the header frame and the excitation sources.

2 Materials and methods

2.1 Structure and working process of full-feeding rice combine

A certain model of full-feeding rice combine harvester is widely used in many cultivation areas in China. The structure of the machine is shown in Figure 1. It is mainly composed of header assembly, tilt conveyor, threshing device, cleaning device, unloading auger, grain tank, and other working parts as well as relevant accessories such as hydraulic system. The wide track wheel and deep mud feet paddy field power chassis can ensure sufficient touchdown area and good trafficability in the complex paddy field environment. The width of the header is 2000 mm, which can meet the requirements of efficient harvest in the field. Stepless adjustable reel and angle adjustable reel spring teeth can effectively reduce header loss and improve the adaptability of harvesting lodging crops. The combined configuration of the axial threshing cylinder and sieve has the advantages of clean threshing and small cleaning loss. The specific technical parameters are listed in Table 1.



1. Reel 2. Divider 3. Auger 4. Header frame 5. Tilt conveyor 6. Cab 7. Grain tank 8. Unloading auger 9. Threshing device 10. Cleaning device 11. Power chassis

Figure 1 Structure of full-feeding rice combine harvester

Table 1 Technical parameters of full-feeding rice combine harvester

Parameters	Value
Overall dimension/mm×mm×mm	5130×2470×2750
Rated power/kW	75
Track width/mm	450
Header width/mm	2000
Ground clearance of chassis/mm	672
Threshing cylinder/mm×mm	φ620×1960
Sieve/m ²	1.24
Reel diameter/mm	φ900
Feed rate/t·h ⁻¹	16.2
Operation speed /km·h ⁻¹	0-4.8

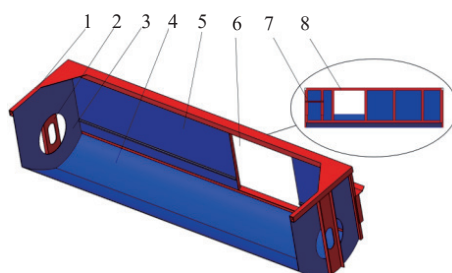
During the harvesting, the divider separates the rice to be cut from the uncut rice, and the reel guides the rice to be cut to the cutter so that the cut rice is laid on the header frame, and the tilted conveyor transports it that is concentrated by the auger to the threshing device. The threshed grains and chaff are sent to the cleaning device composed of the sieve and the cleaning fan for cleaning. And then, the clean grains enter into the grain tank and are unloaded by the unloading auger, and the stalks and sundries are discharged out of the machine, so as to complete the whole harvesting process of rice cutting, conveying, threshing, and cleaning.

2.2 Modal analysis and test of header frame

To find out whether the natural frequencies of header frame were coupled with the frequencies of the excitation source to cause resonance, modal simulation analysis and related research were carried out and their modal characteristics were solved. The accuracy of the finite element model was verified by the combination of the finite element free modal analysis and the free vibration modal test. Constrained modal analysis was used instead of constrained modal test to avoid the dynamic coupling between the working parts and the solution was obtained. The vibration characteristics of the header frame were more accurate and reliable, which provided a reference for the optimization and improvement of the header frame.

2.2.1 Header frame model

The header of a full-feeding rice combine harvester, widely used in China, was taken as the research object. Its frame was 690 mm long and 2000 mm wide along the forward direction. It was mainly composed of square steel, angle steel, and steel plate formed by Q235A structural steel and rigidly connected by welding. In order to reduce the simulation time and ensure the integrity of the structure, we simplified it. 1) Bolt holes fillets far smaller than the grid size, and stamping bars which have less impact on mechanical properties were not considered. 2) Welding flanging which has less impact on the structure and the change of material properties due to welding was ignored. Using 3D software CATIA parameterized the model, as shown in Figure 2.



1. Side members 2. Stiffeners 3. Side walls 4. Floor 5. Rear walls 6. Tilt conveyor inlet 7. Vertical members 8. Beams

Figure 2 Header frame model

2.2.2 Free modal analysis of finite element

The normally basic differential equation of vibration is^[25]

$$M\ddot{x} + C\dot{x} + Kx - P = 0 \quad (1)$$

where, M is the mass matrix of the vibration system; C is the damping matrix; K is the stiffness matrix; P is the external excitation; x is the vibration displacement vector.

For the header frame, the natural frequency is obtained by analyzing the dynamic response of the structure when there is no load, i.e. $P=0$, and the damping of the header frame is very small, which approximately meets $C=0$. The differential equation of undamped elastic vibration is obtained as follows:

$$M\ddot{x} + Kx = 0 \quad (2)$$

The general form of the solution of the equation is

$$x = \varphi e^{j\omega t} \quad (3)$$

where, φ is the corresponding eigenvector; j is the imaginary unit; ω is the natural frequency, Hz; t is the time, s.

Substitute the solution of the equation to get:

$$K\varphi = \lambda M\varphi \quad (4)$$

where, λ is the eigenvalue of the system. The eigenvalues in modal analysis can be obtained if $\lambda = -\omega^2$ is satisfied.

The free modal analysis of finite element mainly studied the natural vibration characteristics of the frame in the free state. The structure was discretized by the finite element method and the mathematical model of its eigenvalues was established. Then the eigenvalues and eigenvectors of the system were calculated by the approximate principle analysis to reflect its vibration frequencies and corresponding modal shapes^[26].

The 3D model of header frame was imported into ANSYS Workbench 18.0 in .STP format for free modal analysis. The header frame can be regarded as a thin-walled structure, which was defined as a shell, and the material was defined as a structural steel (Q235A), whose yield strength was 235 MPa, elastic modulus was 210 GPa, density was 7850 kg/m³, Poisson's ratio was 0.3. In order to make the analysis results more accurate, the cell size set by grid division was 10 mm, and the final total number of cells was 242 896, and the total number of nodes was 479 761. The free mode analysis of finite element does not need to impose constraints, and the first six order rigid body modes with zero frequency will appear^[27]. The low-order vibration had a great influence on the header frame structure, so the non-zero first 8-order modal characteristics were analyzed.

2.2.3 Free modal test

The key of free modal test was modal parameter identification, which was the process of establishing state space expression from test data. The Eigensystem Realization Algorithm (ERA) is to use the multipoint excitation multipoint response method, take the impulse response function as the time domain identification method of the basic model, realize the singular value decomposition of Hankel matrix, and obtain the minimum order system matrix. The following equation is the basic principle of ERA.

Let n -dimensional discrete system state equation:

$$\begin{cases} x(k+1) = Ax(k) + Bu(k) \\ y(k) = Cx(k) \end{cases} \quad (5)$$

where, $x(k)$ is the state vector; $y(k)$ is the observation vector; $u(k)$ is the control vector; K is the sample indicator factor; A is the $n \times n$ dimension state coefficient matrix; B is the $n \times m$ dimension control

coefficient matrix; C is the $p \times n$ dimension observation coefficient matrix.

The system state equation described by Markov parameter (free pulse response function) is as follows:

$$Y(k) = CA^{k-1}B \quad (6)$$

Using the measured free response data $Y(k)$ to construct the normalized Hankel block matrix

$$H_{rs}(k-1) = \begin{bmatrix} Y(k) & \dots & Y(k+t_{s-1}) \\ Y(j_1+k) & \dots & Y(j_1+k+t_{s-1}) \\ \dots & \dots & \dots \\ Y(j_{r-1}+k) & \dots & Y(j_{r-1}+k+t_{s-1}) \end{bmatrix}_{p \times sm} \quad (7)$$

The singular value decomposition of $H_{rs}(0)$ is carried out:

$$H_{rs}(0) = PDQ^T \quad (8)$$

where, P and Q are $r \times p \times n$ dimension left singular vector matrix and $s \times m \times n$ dimension right singular vector matrix respectively; D is $\text{diag}[d_1, d_2, d_3, \dots, d_n]$ $n \times n$ dimension singular value diagonal matrix.

Define:

$$\begin{cases} E_p^T = [I_p, O_p, \dots, O_p], E_m^T = [I_m, O_m, \dots, O_m] \\ P_d = PD, P_d^n = D^{-1}P^T \end{cases} \quad (9)$$

where, I_p and I_m are p and m -order unit matrices respectively; O_p and O_m are p and m -order zero matrices respectively.

Derived:

$$Y(k-1) = E_p^T H_{rs}(k) E_m = E_p^T P D^{1/2} [D^{-1/2} P^T H_{rs}(1) Q D^{-1/2}]^k D^{1/2} Q^T E_m \quad (10)$$

Through comparison, it can be got that

$$\begin{cases} A = D^{-1/2} P^T H_{rs}(1) Q D^{-1/2} \\ B = D^{1/2} Q^T E_m \\ C = E_p^T P D^{1/2} \end{cases} \quad (11)$$

Solve the eigenvalue Z and eigenvector ϕ of the system state coefficient matrix A ,

$$\phi^{-1} A \phi = Z, Z = \text{diag}[z_1, z_2, \dots, z_n] \quad (12)$$

The relationship between complex parameters considering Laplace transforms and Z transform:

$$S_i = \frac{1}{\Delta\tau} \ln(z_i) \quad (13)$$

where, $i=1, 2, 3, \dots, n$, $\Delta\tau$ is the sample sampling interval.

Obtain modal parameters:

$$\begin{cases} w_i = \text{Im}(s_i) \\ \xi_i = -\text{Re}(s_i)/|s_i| \\ E_p^T P D^{1/2} \phi = C \phi \end{cases} \quad (14)$$

where, w_i is the i order natural frequency; ξ_i is the i order damping ratio; ϕ is the mode matrix.

Through the ERA, the excitation and response of header frame obtained from modal test can be effectively processed, and the natural frequencies, damping ratio, and corresponding modal shapes can be obtained.

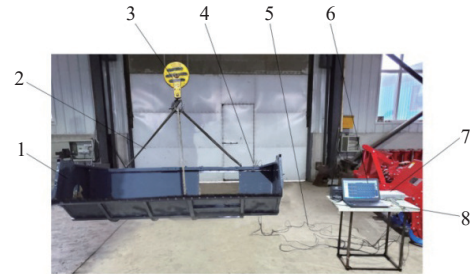
The free modal test was to verify the accuracy of header frame parametric modeling by comparing the results of free mode calculation. In order to identify the modal parameters of the system, the force hammer was used to excite the header frame, and the acceleration sensor was used to pick up the response, which provided the basis for the analysis of vibration characteristics of

structural system and the optimization design of structural dynamic characteristics. There is a relationship between the excitation point and the response point^[28], i.e.:

$$H_{ij}(\omega) = \sum_{i=1}^N \frac{\phi_i \phi_{rj}}{m_r [(\omega_r^2 - \omega^2) + j2\xi_r \omega_r \omega]} \quad (15)$$

where, $H_{ij}(\omega)$ is the transfer function of the system; N is the total order of the identified modes; $\phi_i \phi_{rj}$ is the r order mode shape at points i and j ; m_r is the modal mass; ξ_r is the modal damping ratio; ω_r is the modal frequency.

In the test, in order to ensure that the rigid body modal of the frame was less than 1/3 of the first elastic body modal, the header frame was hoisted with soft rubber rope by means of three-point suspension^[29]. The test equipment consisted of computer, INV3018C 8-channel 24 bit high-precision data acquisition instrument (Beijing Dongfang Institute, Beijing, China), LC-2D force hammer (Beijing Dongfang Institute, Beijing, China), AY100I piezoelectric acceleration sensor (Beijing Dongfang Institute, Beijing, China) and DASP-10 modal analysis system (Beijing Dongfang Institute, Beijing, China). The equipment connection is shown in Figure 3.



1. Header frame 2. Soft rubber rope 3. Lifting ring 4. Acceleration sensor 5. Signal transmission wire 6. Computer 7. Data acquisition instrument 8. Force hammer

Figure 3 Equipment connection diagram

In order to avoid the additional mass effect and to decompose the repetitive modes easily, the multi-input and multi-output (MIMO) method was adopted in this test. LC-2D force hammer was used to excite all measuring points of the whole structure. In order to ensure high signal-to-noise ratio of the hammering signal, the measuring points were arranged to reflect the overall shape of the entity and reflect the external force acting point, structural intersection point, and important response point. Finally, a hammering model with 65 measuring points was established, as shown in Figure 4.

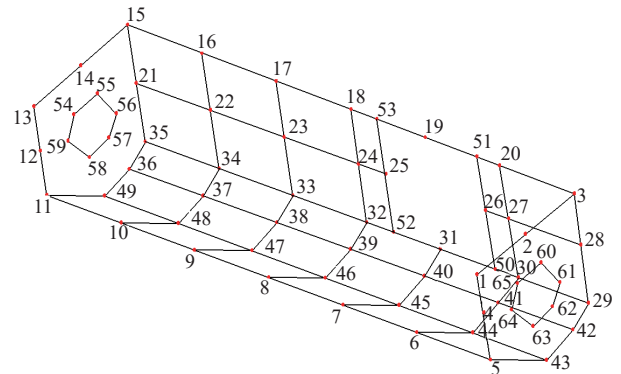


Figure 4 Measuring point model of header frame

The excitation signal of the force sensor on the hammer and the response signal of the piezoelectric acceleration sensor were

transmitted to the data acquisition instrument at the same time. The time-domain signal was decomposed by the singular value of Hankel matrix through the ERA, and the system matrix of the minimum order was obtained, so as to identify the natural frequencies and modal shapes of the structure. The test principle is

shown in Figure 5. Among them, the response point should not only avoid the node but also be placed in a position easy to excite. Finally, the piezoelectric acceleration sensors were arranged at 16, 24, and 38 points on the measurement point model of the rack as the response point to receive signals.

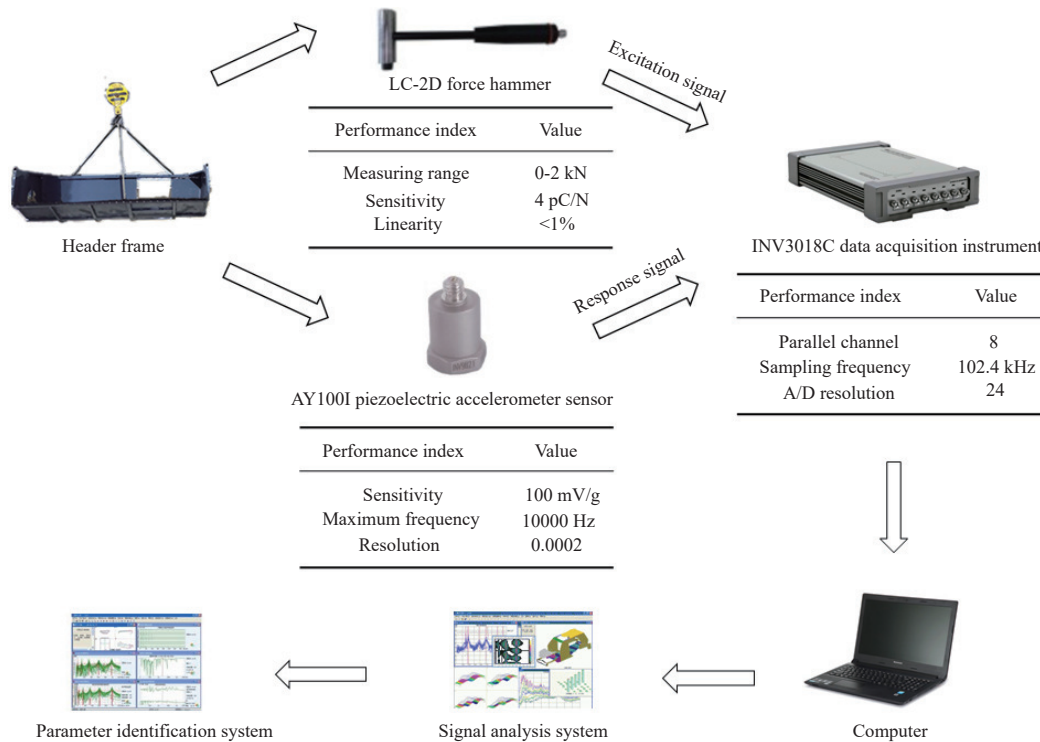


Figure 5 Test schematic diagram

The first eight modal frequencies and modes of the collected signals were extracted by Frequency Response Function (FRF) calculation, impulse response function solution and ERA. In order to verify the mode correlation of the test mode, the Modal Assurance Criterion (MAC) was used for evaluation, and the mode correlation matrix verification is shown in Figure 6. The first mock exam is the correlation coefficient between two vectors. The MAC value of the two vectors of the same physical mode is close to 1, while the MAC value between the two vectors of the different modes is relatively small, which indicates that the two modal vectors are similar to the same mode^[30]. It can be seen from the figure that the correlation coefficient between the diagonal element and its own mode was always 1, and the peak value of the non-diagonal element was less than 0.3 of the threshold value of the discriminant correlation degree, which indicated that the orthogonality between the two vectors was good, the first eight modes of the header frame were independent modes, the test coherence was good, and the results of the modal test parameters were reliable.

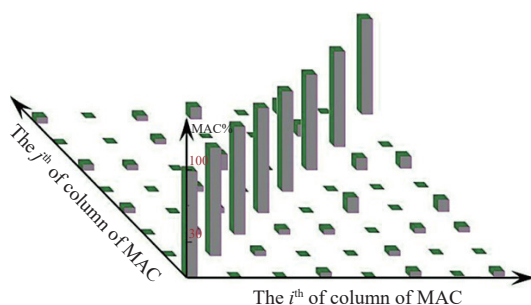


Figure 6 Confidence matrix of modal test analysis

In order to compare the errors of frequency between finite element free modal analysis and modal test, Equation (16) was used.

$$e = \frac{|F_1 - F_2|}{F_2} \times 100\% \quad (16)$$

where, e is the error, %; F_1 is the frequency of finite element free modal analysis, Hz; F_2 is the frequency of modal test, Hz.

2.2.4 Constrained modal analysis of finite element

Based on the accurate model of the header frame, it was imported into ANSYS Workbench. According to the actual constraint state of the header, the fixed boundary conditions were set at the entrance of the tilt conveyor for finite element constrained modal analysis.

2.3 Frequency of excitation source

When the external excitation frequency is close to or equal to the restrained modal frequency of header frame, resonance will occur^[31]. Resonance leads to the transmission, expansion, and radiation of vibration and noise on the machine, which seriously affects the reliability and driving comfort. Under the action of local mode or coupling vibration, it led to the deformation of the weak part, stress concentration, and fatigue damage^[32]. In addition, severe vibration and grain contact led to a large area of header loss, which affected the harvest effect. The engine, threshing cylinder, sieve, and other working parts were installed on the main frame of the combine harvester, whose vibration can be transmitted to the header frame through the main frame. Exploring the factors that affected the vibration of the header frame and analyzed its excitation frequency, and the modal frequencies of each order of the header frame avoided the external excitation frequency, so as to effectively avoid the occurrence of resonance.

1) The engine is the main vibration source of the combine harvester. The vibration comes from the periodic gas pressure in the cylinder and the inertia force produced by the reciprocating motion of the crank. The calculation formula of the excitation frequency is

$$f_1 = \frac{2nz}{60\tau} \tag{17}$$

where, f_1 is the excitation frequency of engine, Hz; n is the engine speed, and its working speed is 2200-2400 r/min; z is the number of engine cylinders; τ is the number of engine strokes. This machine adopts an in-line four cylinder four stroke engine, so z is 4 and τ is 4.

2) The rotary motion of the working parts on the header can also produce violent vibration, such as the rotation of the reel, the rotation of the auger, the reciprocating motion of the cutter, etc., in which the vibration of the cutter mainly comes from the rotary motion of the spatial crank connecting rod slider structure^[33], and the excitation frequency is obtained by converting the crank speed of the cutter. In addition, the rotating working parts that are in contact with the combine frame can also transmit the vibration on the frame, such as the threshing cylinder and the crankshaft of the sieve. The rotating speed was measured by RM-1000 photoelectric tachometer (Shanghai TES Electronics Co., Ltd., Shanghai, China).

The formula for calculating the excitation frequency of rotating working parts is

$$f_2 = \frac{n}{60} \tag{18}$$

where, f_2 is the excitation frequency of rotating working parts, Hz; n is the rotation speed, r/min. The rotation speed of reel is 40-55 r/min, the rotation speed of the cutter crank is 400-450 r/min, the rotation speed of the auger is 145-180 r/min, the rotation speed of the threshing cylinder is 700-800 r/min, the excitation frequency of the

sieve is caused by the reciprocating motion, and the rotation speed of the crank driving shaft of the sieve is 350-400 r/min.

3) The road conditions of the harvester are mostly rural roads and paddy fields after drying, and the combine harvester has a good vibration isolation effect by contacting the ground through the track with small rigidity. Its excitation frequency is generally 0-3 Hz^[34].

According to the resonance theory, resonance occurs when the natural frequency of the structure has the following relationship with the external excitation frequency^[35], that is

$$0.8f_c \leq f \leq 1.2f_c \tag{19}$$

where, f_c is the natural frequency of the structure, Hz; f is the external excitation frequency, Hz.

2.4 Topology optimization of header frame

Taking the first-order and eighth-order frequencies as the optimization objective and different mass fraction as the constraint condition in ANSYS Workbench 18.0, topology optimization was carried out. In the process of rice harvest, the pressure of screw conveyor on rice was all acting on the floor. In topology optimization, the material of floor was reserved, and the remaining parts such as side walls, stiffeners and rear walls were taken as optimization areas to explore the influence on the modal frequency of header. In order to obtain a reasonable and reliable topology of header frame, and to control the checkerboard phenomenon, avoid small force transfer path and material accumulation, which makes the complexity of the optimized configuration larger, three times of the size when dividing the grid was taken as the minimum member size, and six times of the size was taken as the maximum size. That was, the minimum member size was 30 mm and the maximum member size was 60 mm. The topology optimization model with 10%-90% mass fraction constraints is shown in Figure 7.

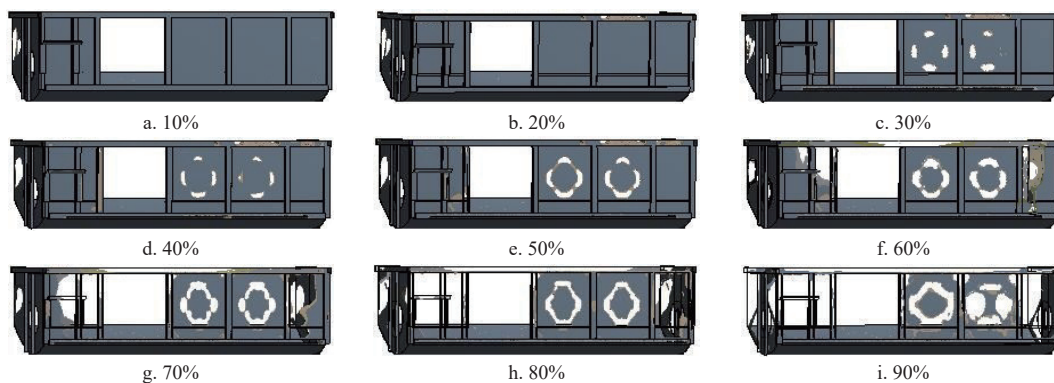


Figure 7 Topology optimization with different mass fraction constraints

If the density exceeds the set threshold value after optimization iteration, no material will be displayed. Through the gradual iteration of different mass constraints, it can reflect the influence of specific structural position on the frequencies of header frame. Figure 7 shows that the side walls of header frame first have a large area of material deletion, which indicates that the side wall material has a great influence on improving the frame frequency during the optimization process. Some materials of the rear walls have also been deleted, and then the rear wall material has a second effect on the frame frequency after the side wall. In the mold reconstruction, the addition and deletion of the side wall material and the change of the rear wall material need to be considered.

In order to explore the change rule of strength and rigidity of header frame after topology optimization under different mass constraints, the static analysis and average frequency analysis were

carried out. Among them, the static analysis mainly checked the strength and rigidity of the frame under different mass constraints. The frame had its own gravity, and at the same time received the gravity load of the components installed on it. There are still some hydraulic pipelines and other auxiliary parts on the header, but the mass of auxiliary parts can be ignored compared with that of other parts. The volume of each part of header was obtained by Creo 2.0 software, and the mass of each part was obtained by material density and converted into weight. The external load on the frame was simplified as equivalent load and loaded to the corresponding part of the frame, and the static simulation analysis was carried out. The load on the frame and the loading mode are listed in Table 2.

2.5 Field experiment

In October 2019, a comparative field experiment of rice harvest was conducted in the rice experimental area of Qing'an County,

Table 2 Load of header frame

Load	Type	Load level/N	Application position
Reel	Concentrated force	652	Side member left and right
Auger	Concentrated force	430	Stiffener left and right
Cutter	Uniform force	284	Front end of floor
Transmission parts	Concentrated force	230	Side wall left

Suihua City, Heilongjiang Province. The experiment mainly included two parts: one was to compare whether the vibration of header frame decreases before and after optimization, and the other was to determine whether the header frame increases the header loss after optimization. The two experiments can be carried out at the same time without mutual influence. The experimental area had flat ground and upright rice without lodging. Longjing 29 was a rice variety. Its natural properties were as follows: height was 73.3 cm, 1000 grain weight was 37.7 g, the ratio of grain to grass was 1.06, moisture content of stem was 27.6%-32.4%, moisture content of grain was 13.5%-16.6%, and there was no natural seed dropping. The advance distance of each experiment was 200 m, and 10 m of crops were reserved in front of the experiment area to ensure that the harvester can work stably before entering the experiment area. The height of header was 30 cm, and the engine speed was 2300 r/min to ensure that the operating parameters of all working parts such as driving speed and reel speed were unchanged.

The field experiment is shown in Figure 8. Place the measuring point near the excitation source of header frame prone to vibration radiation, and use INV9832-50 acceleration sensor (Beijing Dongfang Institute, Beijing, China) to collect the vibration characteristics in *X* (forward direction), *Y* (left and right direction) and *Z* (vertical direction)^[36], and the position of the measuring point is shown in Figure 9.

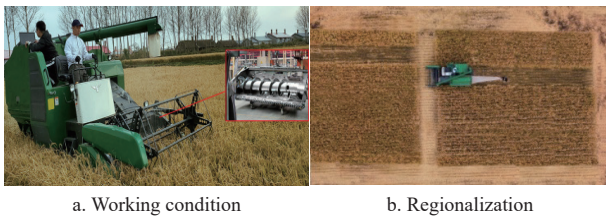
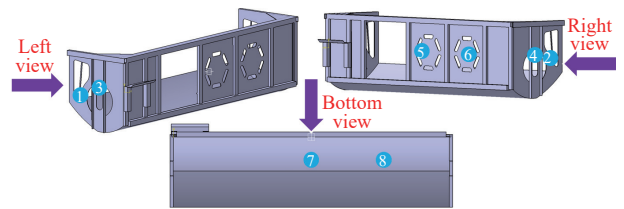


Figure 8 Field experiment

During the experiment, the sampling method was set as continuous sampling, the sampling frequency was 2 kHz, the analysis frequency was 625 Hz, the number of time-domain points was 4096, the number of frequency-domain lines was 1600 and the average number was 10.

The vibration signal of each measuring point was collected three times, and a group of data with the best effect was taken for analysis. The total vibration amount of each measuring point can be



Note: Measuring point 1 is 1/3 of the side wall left; Point 2 is 1/3 of the side wall right; Point 3 is 1/2 of the stiffener left; Point 4 is 1/2 of the stiffener right; Point 5 is 1/2 of the rear wall; Point 6 is 1/3 of the rear wall; Point 7 is 1/2 of the floor; Point 8 is 1/3 of the floor.

Figure 9 Measuring point position of header frame in field experiment

expressed by the root mean square value of vibration acceleration^[37].

$$a = \sqrt{\frac{a_x^2 + a_y^2 + a_z^2}{3}} \tag{20}$$

where, *a* is the Root Mean Square (RMS) value of vibration acceleration of each measuring point, m/s²; *a_x*, *a_y*, and *a_z* are the peak values of vibration acceleration in *X*, *Y*, and *Z* directions of each measuring point, m/s².

In order to further verify whether the optimized header frame increases header loss due to the sealing problem, two nylon mesh bags were fixed on the rice stalk outlet and the tail of the cleaning screen with bolts to collect the residue after straw crushing, so as to eliminate the interference of threshing loss and cleaning loss and ensure the accuracy of header loss measurement. By manually picking up the grain weight and header loss of header frame before and after optimization in an area of 20 m²^[38], repeat the experiment three times to get the average value.

3 Results and discussion

3.1 Vibration characteristics of header frame

Table 3 shows the comparison between the results of finite element free modal analysis and free vibration modal test. The results showed that the eighth-order modal shapes were consistent and the natural frequency error was small. The main causes of the errors were as follows: 1) the dynamic stiffness of the system was increased to a certain extent by some welding spots on the header frame, which was the main reason for the larger frequency error of modal calculation; 2) In the initial stage of the model, the weight of the pores had little influence on the model, and some accessories such as bolts and damping materials were ignored; 3) The structure discretization, iterative calculation, signal acquisition, and processing all produced inevitable errors; 4) The header frame was hoisted with soft rubber rope to ensure that the rigid body mode of the frame was less than 1/3 of the first elastic body mode, which was approximate to the free state but not the absolutely free state. 5) The header frame was large in volume, the impact force of the

Table 3 Comparison between free modal analysis of finite element and free modal test

Order	Free modal analysis of finite element		Free modal test		Error/%
	Calculated frequency/Hz	Vibration mode	Test frequency/Hz	Vibration mode	
1	15.58	Local bending deformation of the floor	15.52	Consistent	0.39
2	27.23	Overall bending, vertical members deformation	26.44	Consistent	2.99
3	33.69	Overall bending, beams deformation	34.37	Consistent	1.98
4	37.77	Local bending of the floor, rear walls deformation	38.78	Consistent	2.60
5	42.37	Local torsional bending deformation of the floor	42.51	Consistent	0.33
6	56.63	Overall bending, Torsional Deformation of the floor and vertical members	54.05	Consistent	4.78
7	58.79	Local bending deformation of the floor	60.26	Consistent	2.89
8	69.24	Local torsional bending deformation of the floor	71.37	Consistent	2.98

force hammer generating the excitation was relatively small, and part of the energy transmitted from the excitation point to the response point was seriously attenuated. However, within the allowable error range, the established finite element parametric model was accurate and reliable, which laid a foundation for further finite element constrained modal analysis.

It can be seen from Figure 10, the frequency range of the eighth-order constrained modal is 13.20-79.64 Hz, and the modal frequencies of each stage are significantly different from those of the free modal. Refer to the data in comparison Table 4 and Figure 9 for the difference. The constrained modal frequency can more accurately reflect the vibration characteristics of the structure, which was consistent with the research results of Chen et al.^[39] Because of the large size and small rigidity of the header of the combine harvester, the constrained modal vibration mode mainly showed the local torsion and deformation of the floor and side

walls. Since the outer edge of the header floor needed to be connected with the cutter device, the failure to install the stiffener leads to large deformation in the third, sixth, and seventh modal shapes. While the side walls are in the weak link that crosses the divider installation, resulting in local deformation. The fifth and eighth modal shapes were the overall modal of the header frame. Therefore, the side walls were the main part of the structural vibration and radiated noise of the header, which should be considered in the optimization and improvement.

In this study, the accuracy of the finite element model of the header frame was verified by free modal analysis and free vibration modal test, and the modal shapes and frequencies of the constraint modal are solved at the same time. This method can provide a beneficial reference for accurately obtaining the natural frequency of the constraint state when solving structural vibration characteristics.

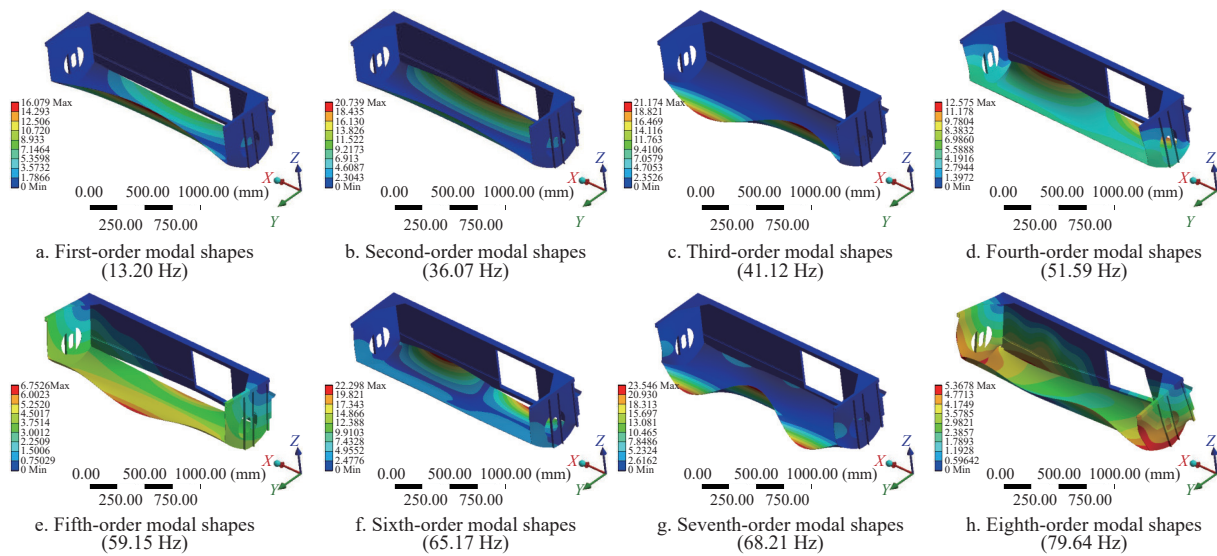


Figure 10 Constrained modal shapes and corresponding frequencies

Table 4 Frequency excitation source

Excitation source	Frequency/Hz
Engine	73.33-80
Reel	0.67-7.50
Cutter	6.67-7.50
Auger	2.42-3
Threshing cylinder	11.67-13.33
Sieve	5.83-6.67
Ground	0-3

3.2 Resonance analysis with multi-source excitation

The frequency of each excitation source is listed in Table 4. When the frequency of the excitation source was close to the natural frequency of each stage of the header frame, resonance occurred.

According to the analysis of the excitation source of the header, the first-order modal frequency was 13.20 Hz, which was in the range of 11.67-13.33 Hz of the threshing cylinder, and they are prone to resonance. The eighth-order modal frequency was 79.64 Hz in the range of 73.33-80.00 Hz of the engine, and they were prone to resonance. Therefore, it was necessary to optimize the header frame, improve its first and eighth order modal frequencies to avoid the excitation frequency of the threshing cylinder and engine, and ensure that other modals do not have frequency exchange phenomenon to avoid resonance effectively.

Due to the different materials used in the working parts and the non-circular rotation caused by the wear between the contact surfaces of the rotating parts, the vibration will increase. When the excitation sources work at the same time, some non-rotating parts will vibrate. These vibrations have a certain frequency. When the vibration frequency is coupled with the natural frequency of the header frame, they will also become the excitation sources of the header frame. The interaction of the excitation sources is complex, and cannot be directly obtained by calculation or test, and the contribution of vibration is different. In the later stage, we will carry out the blind source identification and analysis of the excitation force by using the principal component analysis method, and focus on the influence of the signal-to-noise ratio, the distribution of measuring points, and the number of measuring points on the principal component power spectrum, contribution rate, cumulative contribution rate and the number of excitation sources, in order to get the primary and secondary relationship between the coupling effects of various excitation sources.

3.3 Analysis of topology optimization results

3.3.1 Static analysis of different mass fraction constraint

The maximum stress under different mass fraction constraints is shown in Figure 11, and its maximum stress directly reflects the strength of header frame. The regression equation in Figure 10 is used to analyze and predict the relationship between maximum

stress and removal. R^2 represents the overall fit of the regression equation. The maximum value of R^2 is 1. The greater R^2 , the better the fitting degree of the regression equation. With the increase of the mass fraction constraint in the process of topology optimization, the maximum stress tended to stabilize first and then increase. Because the various reinforcement beams of the header frame played a skeleton and load-bearing role, the side walls and the rear walls were not effective areas for carrying working parts. When the mass fraction constraint was from 10% to 50%, only the side walls and the destruction of some materials from the rear walls do not cause damage to various skeleton beams, resulting in a steady trend in the maximum stress and a small increase, which did not affect the overall strength of the structure. When the mass fraction constraint was greater than 50%, the maximum stress growth trend increased obviously. When the mass fraction constraint was 60%, the maximum stress was 240.9 MPa, which exceeded the allowable stress 235 MPa of the frame. The side members and beams of the header frame were damaged one after another and sharp openings appeared, resulting in stress concentration. The larger reel load and anger were respectively loaded on the side members and stiffeners, the header frame as a whole cannot bear its pressure, and the strength cannot meet the requirements.

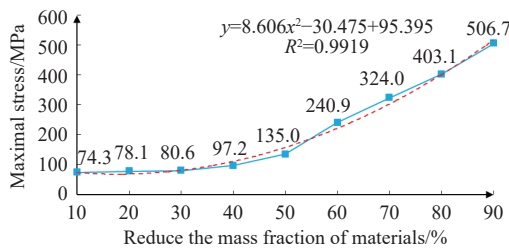


Figure 11 Maximum stress under different mass fraction constraint

The maximum deformation under different mass fraction constraints is shown in Figure 12, and its maximum deformation directly reflects the rigidity of header frame. With the increase of the mass fraction constraint in the process of topology optimization, the maximum deformation tends to stabilize first and then increase. The maximum deformation occurs in the large area of the floor when the fraction constraint was in the range of 10%-50%, mainly because the width of the header floor was large and the skeleton beam was small, the frame structure of the header damaged in this stage does not involve the header floor, and its deformation tended to small and steady rise. When the fraction constraint was more than 50%, the deformation began to increase significantly. The maximum deformation was transferred from the header floor to the side walls, mainly because the side members and other supporting frame beams were damaged one after another. Because the reel was mainly loaded on the left and right sides of the side members, the side walls installed at the lower part of the side members with less rigidity were deformed greatly, while the anger installed at the left and right sides of the stiffeners is deformed greatly. As the mass fraction constraints continue to increase, the removal of materials increased, and its side members, beams, and vertical members were damaged more seriously. The whole header frame can no longer bear the load of reel, anger, and other working parts without the support of framework beam, resulting in the deformation increased to the header frame loss of bearing and protection capacity, and the rigidity can no longer meet the requirements. So when the mass fraction constraint was more than 50%, it was not the best reference for topology optimization.

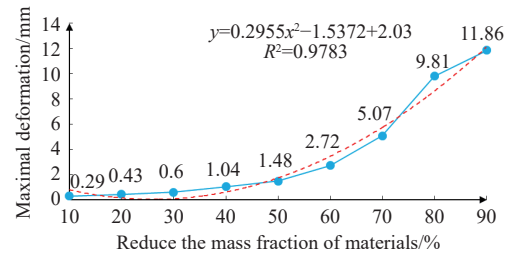


Figure 12 Maximum deformation under different mass fraction constraint

3.3.2 Frequency analysis of different mass fraction constraint

The first and eighth order frequencies under different mass fraction constraints are shown in Figure 13. With the increased mass fraction constraint in the process of topology optimization, the first and eighth order frequencies tended to increase. In this stage, the material of the side walls and the rear walls were mainly removed. Because the side walls and the rear walls were the non-structural concentrated mass that can protect the rice from leakage. With the decrease of the non-structural concentrated mass, the modal frequencies increased gradually.

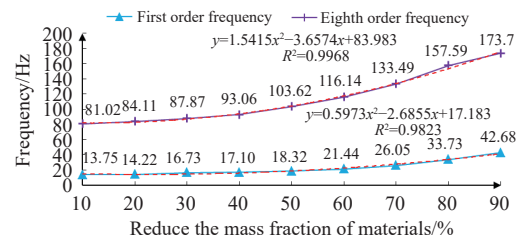


Figure 13 First and eighth order frequencies under different mass fraction constraint

According to the excitation frequencies of threshing drum and engine, the first and eighth natural frequencies of header frame need to be greater than 16.66 Hz and 100 Hz, respectively. It can be seen from Figure 12 that the first-order natural frequency of the header frame need to meet 40% of the mass of the removal optimization area, and the eighth-order natural frequency needs to meet 50% of the mass of the removal optimization area to avoid resonance.

Considering synthetically the strength, rigidity, average frequency, and other indexes of header frame after topology optimization, processing and manufacturing factors, and the closeness of the working state of header floor, the topological configuration was geometrically repaired by analyzing its density distribution nephogram, and the topological structure was restored in the working environment of CATIA_V5_R20. Based on 50% of the mass fraction constraint, A trapezoidal hole with an upper bottom of 250 mm, a lower bottom of 400 mm, and a height of 250 mm shall be opened on the side walls. In order to prevent the rice after harvesting from leaking out, a stiffener with a width of 10 mm shall be installed inside the opening. A hexagon groove with a length of 35 mm and a width of 10 mm shall be opened on the two rear walls, In order to avoid the fatigue damage caused by stress concentration, the edges of the opening are all rounded. The reconstructed header frame is shown in Figure 14.

3.4 Comparison of results before and after optimization

In order to verify the optimization effect of the reconstructed header frame model, ANSYS Workbench 18.0 was used to carry out static and modal analysis of the header frame before and after the optimization, as listed in Table 5.

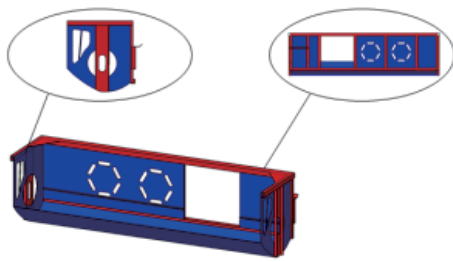


Figure 14 Reconstructed header frame model

Table 5 Performance comparison of header frame before and after topology optimization

Optimization situation	Mass/kg	Maximum stress/MPa	Maximum deformation/mm
Before optimization	96.16	70.6	0.37
After optimization	82.53	128.6	0.42

Topology optimization aims at increasing the average frequency and taking into account the lightweight design. Its quality was reduced by 14.17%. Because the maximum stress and maximum deformation of header frame will inevitably increase

after material removal, the maximum stress of 128.6 MPa was far lower than the fatigue failure stress of 235 MPa, which met the strength requirements. The maximum deformation of 0.42 mm still belonged to the small deformation category and meets certain rigidity requirements. The modal analysis was carried out. The eighth-order restrained modal frequencies and modes are shown in Figure 15.

The range of the 8-order constrained modal frequencies were 17.83-101.59 Hz after optimization, and the main vibration modal shapes were the local torsion and deformation at the installation of the header floor cutter. Because of the hole structure in the rear walls, the mass and stiffness distribution change, which led to the whole rear walls and had no vibration displacement. Before optimization, the side walls with large vibration displacement also have obvious improvement. The first three modal shapes had a great influence on the overall structure and did not have vibration, and the maximum displacement of the fourth modal shape was only 0.11 mm. The eighth-order modal shapes behaved as the overall mode before optimization, while the overall mode changed to the local mode after optimization, and the overall performance was better than that before optimization.

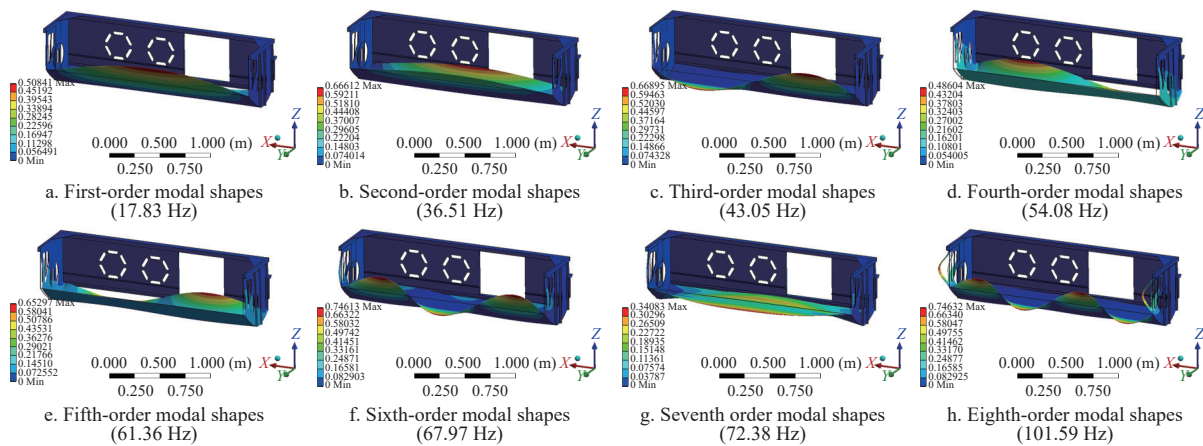


Figure 15 Constrained modal shapes and corresponding frequencies after optimization

It can be seen from Table 6 that after optimization, the frequencies of each order were improved to different degrees, among which the first and eighth order modal frequencies were obviously improved, from 13.75 Hz and 81.02 Hz to 17.83 Hz and 101.59 Hz, respectively, increasing by 35.08% and 27.56%. The results indicated that the topology optimization effect was significant. The first and eighth order natural frequencies before optimization were within the excitation frequency range of threshing cylinder and engine respectively, which were easy to resonate. The first and eighth natural frequencies were far away

from the excitation frequency range of threshing cylinder and engine, other modal frequencies did not exchange and were far away from the range of excitation frequencies, which showed that the resonance was effectively avoided after topology optimization.

In this study, the vibration characteristics of the header frame were studied and the excitation frequencies were far away from the threshing cylinder and the engine to reduce the resonance. By analyzing the vibration characteristics of the excitation source, blocking the vibration transmission or optimizing the structure of the excitation source to keep its frequencies far away from the natural frequencies of the research object, the resonance can also be avoided. For example, the engine was the main source of excitation that affects the vibration of the tractor^[40], and the transmission of the unbalanced inertia force of the engine on the tractor can be effectively reduced by installing a vibration isolator between the tractor engine and the chassis^[41,42]. In addition, the topology optimization method is used to optimize the header frame to reduce resonance and realize lightweight design, which provided lightweight design basis for reducing the vibration of header frame, and provide reference for other types of machinery in the field of agricultural machinery to reduce weight and vibration. Some scholars got the optimal structure through the combination of multi-objective topology optimization such as stiffness and frequency, and

Table 6 Natural frequencies comparison before and after optimization

Order	Before optimization/Hz	After optimization/Hz	Variation/Hz	Variation ratio/%
1	13.20	17.83	4.63	35.08
2	36.07	36.51	0.44	10.22
3	41.12	43.05	2.39	5.81
4	51.59	54.08	2.49	4.83
5	59.15	61.36	2.21	3.74
6	65.17	67.97	2.80	4.30
7	68.21	72.38	4.17	6.11
8	79.64	101.59	21.95	27.56

the combination of topology optimization and shape optimization, and other optimization methods had also achieved good optimization results^[43-46]. In the later stage, based on the multi-objective topology optimization, combined with a variety of optimization methods, we will focus on the research of weight reduction and vibration reduction of key components of combine harvester, in order to broaden new optimization channels and methods for key components of agricultural machinery.

3.5 Results of field experiment

The peak value and RMS value of vibration acceleration in three directions of each measuring point are listed in Table 7.

Table 7 Peak acceleration comparison of field experiment before and after optimization

Measuring point	Before optimization				After optimization			
	Peak vibration acceleration/m s ⁻²			RMS/m s ⁻²	Peak vibration acceleration/m s ⁻²			RMS/m s ⁻²
	X	Y	Z		X	Y	Z	
1	12.32	19.12	10.86	14.55	9.32	13.72	7.75	10.57
2	12.77	18.55	10.91	14.45	9.62	14.43	8.13	11.06
3	9.62	13.29	9.49	10.94	4.32	5.77	5.16	5.12
4	9.41	12.80	9.67	10.74	4.48	5.68	4.98	5.07
5	26.45	23.87	21.99	24.17	6.00	8.83	6.30	7.16
6	23.14	18.76	20.47	20.87	5.54	8.74	5.91	6.88
7	4.42	5.86	8.67	6.56	3.44	3.56	6.62	4.77
8	4.01	5.49	7.57	5.87	3.51	3.27	5.23	4.10

In the field experiment, because of the good soft damping effect of paddy field and the good vibration isolation effect of wide track wheel, the random excitation of the ground had little effect on the header frame, which can be ignored. It can be seen from Table 7 that the peak value of vibration acceleration before optimization was relatively large in all directions, and the RMS value of vibration acceleration at measuring point 5 was 24.17 m/s². Mainly due to the resonance phenomenon caused by the vibration coupling between the excitation frequency of the engine and the threshing cylinder with large load and the natural frequency of the header frame. The header frame was an axisymmetric mechanism, and measuring points 1 and 2 showed that there was little difference in the peak value and the RMS value of vibration acceleration in the three directions of X, Y, and Z when measuring points are arranged symmetrically on the left and right side walls. The peak value in Y direction was significantly higher than that in X and Z directions, which indicated that the inertia force of the cutter still affect the vibration in Y direction close to the cutter even if the reciprocating motion of the cutter does not cause resonance of the header frame. It cannot be avoided after optimization, which was a common problem of the reciprocating cutter. The effect of Y direction vibration can be reduced by adding appropriate control parameter balance block on the crankshaft^[47]. Measuring points 3 and 4 were placed at the stiffeners on the left and right sides. Since the stiffeners were fixed on the side walls of header frame, they were equivalent to the thickened side walls, and their overall vibration acceleration peaks were smaller than the side walls. The rear walls were obviously affected by resonance. Since 1/2 of the rear walls were longer than 1/3 of the rear walls from the fixed position of the framework, the overall vibration of measuring point 5 was greater than that of measuring point 6. Measuring points 7 and 8 respectively measured the vibration acceleration of the floor of the header frame, and the peak value was smaller than that of other measuring points. The reason was that in the experiment, the feeding rate was uniform at the normal harvesting speed, the load

fluctuation was small, and the rice was filled with the gap between the screw pusher and the bottom plate, resulting in the rice absorbing part of the vibration. After topology optimization, the peak value of vibration acceleration and the RMS value of vibration acceleration of each measuring point were reduced to different degrees. The RMS values of vibration acceleration of measuring points 5 and 6 with obvious vibration are reduced by 70.38% and 67.03% respectively, and no violent vibration occurred in the harvesting process. Field experiment showed that topology optimization can effectively reduce the amplitude of header frame and avoid resonance.

Before optimization, the grain yield was 36.28 kg, the header loss was 303.64 g, and the header loss rate was 0.83%. After optimization, the grain yield was 34.60 kg, the header loss rate was 268.49 g, and the header loss rate was 0.77%. The results showed that the optimized header frame does not increase the header loss. It was possible that because the rated engine speed of combine harvester is forward and its feeding amount was uniform, a large amount of straw after harvesting by cutter was intertwined with each other under the action of screw conveyor and telescopic finger, which can form a certain protection for rice panicle head and do not thresh at the header. The small-scale hole digging design of header side wall and rear mounting plate do not cause grain leakage and increase header loss.

When the natural properties of crops are the same, header loss is mainly related to cutter speed, reel speed, travel speed, etc. The fully-feeding rice combine harvester adopts the reciprocating cutter. The cutting speed of this kind of cutter is small, which will cause the rice straw with small rigidity to be pushed down or missed and the straw to tilt and shake, resulting in a large header loss^[48], and the cutting distance is generally controlled at 60-80 mm during the working. When the speed of the reel is high, the impact on the ear of the crop will be intensified, resulting in a sharp increase in header loss, and the speed ratio of the reel is generally 1.5-1.6^[49]. Therefore, in the design of header loss verification experiment, it is necessary to ensure that the engines of each group of tests work at rated speed and keep consistent so that the cutter speed, reel speed, and traveling speed reach the best, the inconsistency of working parameters of working parts shall be avoided to interfere with the verification of header frame sealing and affect the experiment results.

4 Conclusions

Based on the analysis and optimization of the vibration characteristics of the header frame, the research conclusions were as follows:

1) The natural frequency and external excitation frequency of the header were analyzed. The first-order modal frequency of the header frame was 13.20 Hz within the range of 11.67-13.33 Hz of the excitation frequency of the threshing drum, and the eighth order modal frequency was 79.64 Hz within the range of 73.33-80 Hz of the engine excitation frequency, which was prone to resonance.

2) The optimized header frame met the strength and stiffness requirements, and the first and eighth modal frequencies were increased by 35% and 22.5% respectively, avoiding resonance.

3) After optimization, the mass of header frame was reduced by 14.17%, and the root mean square values of vibration accelerations at measuring points 5 and 6 were reduced by 70.38% and 67.03% respectively. This study provides an effective reference for weight reduction and vibration reduction of the header frame of rice, wheat, rape, and other crop combine harvesters.

Acknowledgements

This work was financially supported by the Program on Industrial Technology System of National Rice (CN) (CARS-01-48).

[References]

- [1] Hu Q, Jiang W Q, Qiu S, Xing Z P, Hu Y J, Guo B W, et al. Effect of wide-narrow row arrangement in mechanical pot-seedling transplanting and plant density on yield formation and grain quality of japonica rice. *J Integr Agric*, 2020; 19(5): 1197–214.
- [2] Xing Z P, Wu P, Zhu M, Qian H J, Hu Y J, Guo B W, et al. Temperature and solar radiation utilization of rice for yield formation with different mechanized planting methods in the lower reaches of the Yangtze River, China. *J Integr Agric*, 2017; 16(9): 1923–1935.
- [3] Geng L X, Li K, Pang J, Jin X, Ji J T. Test and analysis of vibration characteristics of transplanting machine based on time frequency and power spectral density. *Transactions of the CSAE*, 2021; 37(11): 23–30. (in Chinese)
- [4] Wang W Z, Lu H Z, Zhang S M, Yang Z. Damage caused by multiple impacts of litchi fruits during vibration harvesting. *Computers and Electronics in Agriculture*, 2019; 162: 732–738.
- [5] Du X Q, Jiang F, Li S T, Xu N N, Li D W, Wu C Y. Design and experiment of vibratory harvesting mechanism for Chinese hickory nuts based on orthogonal eccentric masses. *Computers and Electronics in Agriculture*, 2019; 156: 178–186.
- [6] Liu T H, Luo G, Ehsani R, Toudeshki A, Zou X J, Wang H J. Simulation study on the effects of tine-shaking frequency and penetrating depth on fruit detachment for citrus canopy-shaker harvesting. *Comput Electron Agric*, 2018; 148: 54–62.
- [7] Castro-García S, Sola-Guirado R R, Gil-Ribes J A. Vibration analysis of the fruit detachment process in late-season ‘Valencia’ orange with canopy shaker technology. *Biosyst Eng*, 2018; 170: 130–137.
- [8] He L, Fu H, Karkee M, Zhang Q. Effect of fruit location on apple detachment with mechanical shaking. *Biosyst Eng*, 2017; 157: 63–71.
- [9] Zou T X, Zhang J, Pang J, Li C B, Liu B, Jia W Y, et al. The structure modal analysis and engineering application of the passenger car driver’s seat system. *SAE-China Congress & Exhibition*, 2016; pp.349–363.
- [10] Bajoria K M, Sangle K K, Talicotti R S. Modal analysis of cold-formed pallet rack structures with semi-rigid connections. *J Constr Steel Res*, 2010; 66(3): 428–441.
- [11] Kumar A, Dwivedi A, Jaiswal H, Patil P P. Material-based vibration characteristic analysis of heavy vehicle transmission gearbox casing using finite element analysis. *Adv Intell Syst Comput*, 2015; 308(1): 527–533.
- [12] Jin X, Chen K K, Ji J T, Pang J, Gao S, Zeng X Y. Modal analysis and structure optimization of transplanter support arm based on modal assurance criterion. *Transactions of the CSAE*, 2018; 34(18): 93–101. (in Chinese)
- [13] Tang Z, Zhang H T, Zhou Y P. Unbalanced vibration identification of tangential threshing cylinder induced by rice threshing process. *Shock Vib*, 2018; 2018: 4708730.
- [14] Yao Y C, Song Z H, Du Y F, Zhao X Y, Mao E R, Liu F. Analysis of vibration characteristics and its major influenced factors of header for corn combine harvesting machine. *Transactions of the CSAE*, 2017; 33(13): 40–49. (in Chinese)
- [15] Deboli R, Calvo A, Preti C. Whole-body vibration: Measurement of horizontal and vertical transmissibility of an agricultural tractor seat. *Int J Ind Ergon*, 2017; 58: 69–78.
- [16] Deprez K, Moshou D, Anthonis J, Baerdemaeker J De, Ramon H. Improvement of vibrational comfort on agricultural vehicles by passive and semi-active cabin suspensions. *Comput Electron Agric*, 2005; 49(3): 431–40.
- [17] Cheng J, Chi R J, Mao E R. Influence of hanging farm implement on vibration of tractor with electro-hydraulic hitch system. *Transactions of the CSAE*, 2015; 31(7): 24–32. (in Chinese)
- [18] Jiang Y J, Liao Y T, Qin C, Guan Z H, Liao Q X. Vibration analysis and improvement for frame of 4SY-29 typed rape windrower. *Transactions of the CSAE*, 2017; 33(9): 53–60. (in Chinese)
- [19] Li Y M, Li Y W, Xu L Z, Hu B Y, Wang R. Structural parameter optimization of combine harvester cutting bench. *Transactions of the CSAE*, 2014; 30(18): 30–37. (in Chinese)
- [20] Yan K, Cheng G D, Wang B P. Topology optimization of damping layers in shell structures subject to impact loads for minimum residual vibration. *J Sound Vib*, 2018; 431: 226–47.
- [21] Xu D K, Chen J, Tang Y C, Cao J. Topology optimization of die weight reduction for high-strength sheet metal stamping. *Int J Mech Sci*, 2012; 59(1): 73–82.
- [22] Kim S I, Kang S W, Yi Y S, Park J, Kim Y Y. Topology optimization of vehicle rear suspension mechanisms. *Int J Numer Methods Eng*, 2018; 113(8): 1412–1433.
- [23] Qin H X, Yang D Q. Vibration reduction design method of metamaterials with negative Poisson’s ratio. *J Mater Sci*, 2019; 54(22): 14038–14054.
- [24] Stanford B, Beran P, Bhatia M. Aeroelastic topology optimization of blade-stiffened panels. *J Aircr*, 2014; 51(3): 938–944.
- [25] Yao Y C, Du Y F, Zhu Z X, Mao E R, Song Z H. Vibration characteristics analysis and optimization of corn combine harvester frame using modal analysis method. *Transactions of the CSAE*, 2015; 31(19): 46–53.
- [26] Tinoco H A, Ocampo D A, Peña F M, Sanz-Urbe J R. Finite element modal analysis of the fruit-peduncle of *Coffea arabica* L var Colombia estimating its geometrical and mechanical properties. *Comput Electron Agric*, 2014; 108: 17–27.
- [27] Wang B T, Cheng D K. Modal analysis by free vibration response only for discrete and continuous systems. *J Sound Vib*, 2011; 330(16): 3913–3929.
- [28] Qin Z Y, Yang Z B, Zu J, Chu F L. Free vibration analysis of rotating cylindrical shells coupled with moderately thick annular plates. *Int J Mech Sci*, 2018; 142–143: 127–139.
- [29] Orlovitz E, Brandt A. Comparison of experimental and operational modal analysis on a laboratory test plate. *Meas J Int Meas Confed*, 2017; 102: 121–130.
- [30] Xu Y F, Zhu W D. Operational modal analysis of a rectangular plate using non-contact excitation and measurement. *J Sound Vib*, 2013; 332(20): 4927–4939.
- [31] Sorokin V, Blekhan I. On the stochastic resonance phenomenon in parametrically excited systems. *Eur J Appl Math*, 2019; 30(5): 986–1003.
- [32] Kang T H, Kaizu Y. Vibration analysis during grass harvesting according to ISO vibration standards. *Comput Electron Agric*, 2011; 79(2): 226–35.
- [33] Pang J, Li Y, Ji J, Xu L. Vibration excitation identification and control of the cutter of a combine harvester using triaxial accelerometers and partial coherence sorting. *Biosyst Eng*, 2019; 185: 25–34.
- [34] Molari G, Bellentani L, Guarnieri A, Walker M, Sedoni E. Performance of an agricultural tractor fitted with rubber tracks. *Biosyst Eng*, 2012; 111(1): 57–63.
- [35] Ji J T, Chen K K, Jin X, Wang Z Y, Dong B Q, Fan J Y, et al. High-efficiency modal analysis and deformation prediction of rice transplanter based on effective independent method. *Comput Electron Agric*, 2020; 168: 105126.
- [36] Soleimani B, Ahmadi E. Measurement and analysis of truck vibration levels as a function of packages locations in truck bed and suspension. *Comput Electron Agric*, 2014; 109: 141–147.
- [37] Ma L N, Wei J Y, Huang X M, Zong W Y, Zhan G C. Analysis of harvesting losses of rapeseed caused by vibration of combine harvester header during field operation. *Transactions of the CSAM*, 2020; 51(S2): 134–138, 201. (in Chinese)
- [38] Chaab R K, Karparvarfar S H, Rahmanian-Koushaki H, Mortezaei A, Mohammadi M. Predicting header wheat loss in a combine harvester, a new approach. *J Saudi Soc Agric Sci*, 2020; 19(2): 179–184.
- [39] Chen S R, Han H R, Lu Q. Modal analysis of header for type 4LZ-20 combine harvester. *Transactions of the CSAM*, 2012; 43(S1): 90–94. (in Chinese)
- [40] Taghizadeh-Alisaraei A. Analysis of annoying shocks transferred from tractor seat using vibration signals and statistical methods. *Comput Electron Agric*, 2017; 141: 160–170.
- [41] Li Y, He L, Shuai C G, Wang F. Time-domain filtered-x-Newton narrowband algorithms for active isolation of frequency-fluctuating vibration. *J Sound Vib*, 2016; 367: 1–21.
- [42] Qin W, Shangquan W B, Luo G H, Xie Z C. A method for estimating mount isolations of powertrain mounting systems. *J Sound Vib*, 2018; 426: 278–295.
- [43] Sam B, Kathirvel K. Development and evaluation of vibration isolators for reducing hand transmitted vibration of walking and riding type power tillers. *Biosyst Eng*, 2009; 103(4): 427–437.
- [44] Luo Z, Chen L, Yang J, Zhang Y, Abdel-Malek K. Compliant mechanism design using multi-objective topology optimization scheme of continuum structures. *Struct Multidiscip Optim*, 2005; 30(2): 142–154.

- [45] Wang X Y, Shi L P, Dai Q W, Huang W, Wang X L. Multi-objective optimization on dimple shapes for gas face seals. *Tribol Int*, 2018; 123: 216–223.
- [46] Xia Y, Wu Y, Hendriks M A N. Simultaneous optimization of shape and topology of free-form shells based on uniform parameterization model. *Autom Constr*, 2019; 102: 148–159.
- [47] Fukushima T, Inoue E, Mitsuoka M, Okayasu T, Sato K. Collision vibration characteristics with interspace in knife driving system of combine harvester. *Eng Agric Environ Food*, 2012; 5(3): 115–120.
- [48] Chen S R, Zhou Y P, Tang Z, Lu S N. Modal vibration response of rice combine harvester frame under multi-source excitation. *Biosyst Eng*, 2020; 194: 177–195.
- [49] Zhang Z Q, Sun Y F, Liu R J, Zhang M, Li H, Li M Z. Design and test of feed rate monitoring system for combine harvester. *Transactions of the CSAM*, 2019; 50(6): 85–92. (in Chinese)